Vibrations of $H_8Si_8O_{12}$, $D_8Si_8O_{12}$, and $H_{10}Si_{10}O_{15}$ As Determined by INS, IR, and Raman Experiments†

Claudia Marcolli, Philippe Lainé, René Bühler, and Gion Calzaferri*

Department of Chemistry and Biochemistry, University of Berne, Freiestrasse 3, 3000 Berne 9, Switzerland

John Tomkinson*

ISIS Facility Rutherford Appleton Laboratory, Chilton, Didcot, Oxfordshire OX11 0QX, United Kingdom

Received: September 4, 1996⊗

A detailed study of the vibrational structure of the silasesquioxanes $H_8Si_8O_{12}$ and $H_{10}Si_{10}O_{15}$ based on INS, IR, and Raman spectra and on a normal-coordinate analysis is reported. The inelastic neutron scattering (INS) spectrum of crystalline $H_8Si_8O_{12}$ is in good agreement with the optical data and allowed the assignment of optically forbidden transitions. The previously published force field, determined from IR and Raman data of $H_8Si_8O_{12}$ and $D_8Si_8O_{12}$, provided a good fit to the INS frequencies and intensities except in the O−Si−H bending region, which is sensitive to intermolecular interactions. The INS spectrum, a comparison of the Raman spectra of dissolved and solid $H_8Si_8O_{12}$, and published diffraction data were used to analyse the influence of crystal packing. A modified force field was developed which is adapted to crystalline $H_8Si_8O_{12}$ and distinguishes between O−Si−H bending force constants for the axial and the equatorial hydrogen atoms. Excellent agreement with all spectra was thus obtained. This force field was also applied to the INS spectra of $H_{10}Si_{10}O_{15}$ and $D_8Si_8O_{12}$. Based on a normal-coordinate analysis of the INS data, the total mean-square displacements (msd) of the hydrogen atoms of $H_8Si_8O_{12}$ were extracted as well as limits for the total msd of the silicon atoms. The msd's and the neutron diffraction values are in good agreement, showing that no or very little static disorder is present in crystalline $H_8Si_8O_{12}$. Based on the msd's, the lowest internal torsional frequency was estimated to be 41 ± 7 cm^{-1}.

Introduction

Silicon, for a long time confined to material science (traditional glass and electronics industries), has now spread out into all domains of modern chemistry. Oligosiloxanes which have attracted much interest in the past few years[1] are among these silicon-based molecules. Especially promising compounds are the cage-shaped oligosilasesquioxanes[2] of the general formula $(RSiO_{3/2})_{2n}$ (n = 2, 3, 4, ...);[3] their wide use ranges from the preparation of high-performance optical fiber to applications in cosmetics.[4−6] Their attraction stems from the appealing combination of unusual structural features (inorganic moiety) with potentially useful chemical functionalities (organic part). We actually distinguish between organo- or organometallo-functionalized silasesquioxanes (R = alkyl, aryl, halide, or organometallics) and the hydrido species (R = H). The first are discussed as sources for new organosiliceous polymers[7] and as precursors to organolithic macromolecular materials (OMM's)[8,9] or porous hybrid inorganic−organic materials.[10] They are considered as "building blocks" or structuralizing agents for the sol−gel preparation of ceramic or polymeric materials showing specific features reminiscent of the cubic precursors;[11] in the field of supramolecular chemistry, novel octasilasesquioxane-based 3-D cores for dendritic supermolecules have also been described.[12] Metal organic derivatives are involved in the generation of catalysts such as siliceous matrix-encapsulated cobalt carbide nanoparticles (R = $Co(CO)_4$)[13] or in the design of new electrochemical devices (R = ferrocenyl).[14] The hydrido species are exploited for different applications. $H_8Si_8O_{12}$ is used in material technology for SiO_2 film deposition[15,16] and in molecular science as an appropriate starting molecule for synthesizing mono- and higher substituted octanuclear silasesquioxanes.[11,17−24] In addition, hydrosilasesquioxanes can be fruitfully viewed as readily available model compounds for studying specific aspects of zeolites. Several recent approaches to understanding the electronic, vibrational, and crystal structures of infinitely extended zeolite and silicate frameworks involve studying their molecular subunits (such as sodalite[25,26]), related molecules, and clusters.[27−33] Silasesquioxanes fulfill the structural requirements for this purpose as they exhibit polyhedral Si−O skeletons which fit closely characteristic building elements of zeolites; furthermore, they are rather stable molecules which can be thoroughly investigated. Specifically, silasesquioxanes have been used to generate a force field for zeolite A,[28] as models for studying pore-opening vibrations in zeolites[34] and structural distortions in D4R units of zeolites.[32] These systems will become yet more important as the synthesis and characterization of new metallasiloxanes increases the number of suitable molecules with which to model the different kinds of zeolites[35−37] and silica-supported transition-metal complexes or catalysts.[38] There are links to similar cage compounds in which some of the Si are replaced by Al, P, Ga, or Ti.[35,39] Moreover, this series of pseudospherical $(HSiO_{3/2})_{2n}$ compounds offer the opportunities to clarify the subtle but determining role of some driving forces which govern the packing and the cage properties of such highly symmetrical species within the bulk molecular-based materials.

Octahydrosilasesquioxane, $H_8Si_8O_{12}$, can be easily prepared by the hydrolytic polycondensation of $SiHCl_3$ in a biphasic medium. In this reaction, $H_{10}Si_{10}O_{15}$ is also formed as a byproduct[40] and we report an isolation procedure based on sublimation, which represents a useful alternative to the more usual size-exclusion chromatography.[41] Properties of several hydrosilasesquioxanes have been well studied in the last years.

* To whom correspondence should be addressed.
† Dedicated to Prof. Rolf Gleiter on the occasion of his 60th birthday.
⊗ Abstract published in *Advance ACS Abstracts,* January 1, 1997.

S1089-5647(96)02742-3 CCC: $14.00

The crystal structures of $H_8Si_8O_{12}$,[42,43] $H_{10}Si_{10}O_{15}$,[44] and $H_{12}Si_{12}O_{18}$[45] were analyzed in detail, and those of the two isomers of $H_{14}Si_{14}O_{21}$ were reported.[46] Their electronic structure and the Si−H + Y−Z → Si−Y + H−Z reaction mechanism under retention of the cage have been studied.[27] The IR and the FT-Raman spectra of $H_8Si_8O_{12}$ and $D_8Si_8O_{12}$ were measured and analyzed, and a harmonic force field in terms of internal coordinates was determined.[28] It was shown that the force field determined for $H_8Si_8O_{12}$ is appropriate to describe the fundamentals of $H_{10}Si_{10}O_{15}$. Results obtained in these studies led to the notion of ring-opening vibrations, which are an appropriate starting point for the study of pore-opening vibrations in microporous materials.[34] The concept of ring-opening vibrations was recently extended to monosubstituted silasesquioxanes of the type $RH_{2n-1}(SiO_{1.5})_{2n}$, $n = 4, 5$.[47] As $H_8Si_8O_{12}$ is a highly symmetric molecule, 14 fundamental vibrations are optically inactive and yet to be firmly located. Because inelastic neutron scattering (INS) is not subject to optical selection rules, the technique offers the possibility of locating the optically inactive modes and refining the previous force field.

We report in this paper a comparative study between the IR (solution), the Raman (solid state and solution), and the INS (solid state) spectra of $H_8Si_8O_{12}$, as well as a normal-coordinate analysis of the experimental data. This approach allows the assignment of optically forbidden frequencies and the observation of crystal packing influences, mainly on the hydrogen atoms. Based on this analysis the previously developed force field of $H_8Si_8O_{12}$ is modified for crystalline $H_8Si_8O_{12}$ by introducing different O−Si−H bending force constants for the axial and equatorial hydrogen atoms. This force field is then applied to the INS spectra of $H_{10}Si_{10}O_{15}$ and $D_8Si_8O_{12}$. Since the INS spectroscopy is particularly sensitive to displacements of the hydrogen atoms, it gives access to their total mean-square displacements. The total mean-square displacements of the hydrogen atoms can therefore be calculated and compared with the values determined by neutron diffraction. Based on the normal-coordinate analysis and the diffraction data, the frequency of the lowest internal torsion is estimated.

Experimental Section

Synthesis of $H_8Si_8O_{12}$ and $H_{10}Si_{10}O_{15}$. Octa- and decahydrosilasesquioxane, $H_8Si_8O_{12}$ and $H_{10}Si_{10}O_{15}$, were synthesized as described in ref 40. From the resulting mixture of oligohydrosilasesquioxanes, $H_8Si_8O_{12}$ can be directly obtained by recrystallization from *n*-hexane. The purity was >99.5 % (determined by gas chromatography).

Purification of $H_{10}Si_{10}O_{15}$. $H_{10}Si_{10}O_{15}$ cannot be obtained in pure form by recrystallization from the mother mixture of $H_8Si_8O_{12}$ and $H_{10}Si_{10}O_{15}$ and was up to now purified by size-exclusion chromatography.[48] However, a useful alternative is to remove $H_8Si_8O_{12}$ from the mixture by sublimation. Typically, a dried mixture of $H_8Si_8O_{12}$ and $H_{10}Si_{10}O_{15}$ (200 mg, ∼80% $H_{10}Si_{10}O_{15}$) was heated to 85 °C. After 4 h, 175 mg of a crude residue which consisted of 94.8% $H_{10}Si_{10}O_{15}$ remained in the flask. This sublimation step was repeated three times until a purity suitable for sensitive spectroscopic measurements (>99%) was reached.

Synthesis of $D_8Si_8O_{12}$. Deuteration of $H_8Si_8O_{12}$ was performed in accordance with the literature procedure,[28,48] using degassed solvents (Merck, p.a.). In a typical experiment a solution of $H_8Si_8O_{12}$ (400 mg) in pentane (300 mL) was added dropwise to a suspension of Pd/C 10% catalyst (100 mg) in pentane (20 mL), under an inert atmosphere. Before use, the catalyst was heated to 200 °C under vacuum (1 Pa) for 6 h. D_2 bubbling while stirring was carried out for 8 h and the suspension subsequently filtered off with a Millipore filter (type GV, 0.22 μm). The solvent was evaporated and the white solid residue recrystallized from hot cyclohexane. This deuteration step was repeated four times; the completion of deuteration was verified by NMR and FTIR. The final compound showed no remaining Si−H or C−H group (from possibly cocrystallized solvent molecules) signals. A total of 340 mg of crystalline $D_8Si_8O_{12}$ (>99.5 % purity) was obtained.

INS Measurements. The INS spectra were taken on the time-of-flight crystal analyzer spectrometer (TFXA) on the pulsed neutron source ISIS at the Rutherford Appleton Laboratory, Chilton, UK. In this spectrometer a white beam of neutrons illuminates the sample held at 12 m from the neutron source. Some of those neutrons with enough energy to excite vibrations within the sample, and yet having a final energy of about 40 cm^{-1}, will be scattered toward the secondary spectrometer. At this step a separation is made between particles with the correct final energy, which are transmitted to the detectors and all others, which are adsorbed. Data are collected over the entire range of fundamental molecular vibrations, from 20 to 4000 cm^{-1}, with a resolution $\Delta E/E$ 2%. The spectrometer has been described in detail elsewhere.[49]

The samples were contained in an aluminum can and held in a cryostat during data collection; $H_8Si_8O_{12}$ (1 g) was measured for 1 day below 40 K; $H_{10}Si_{10}O_{15}$ (300 mg) was measured for 2 days at 7 K and $D_8Si_8O_{12}$ (330 mg) was measured for 4 days at 4 K. The spectra were corrected for background scattering by subtracting the spectrum of the empty aluminum can in the cryostat. The INS spectrum, of neutron counts versus time of flight, was converted into the conventional scattering law, $S(Q,\omega)$, versus frequency, cm^{-1}, by standard programs.

IR and Raman Spectra. The Raman spectra of the solids and solutions in cyclohexane as well as the IR spectra of solutions in carbon tetrachloride were measured as described elsewhere.[28]

Calculations. The normal-mode calculations were performed by the Wilson GF matrix method[50] using the computer program package QCMP067[51] and the INS spectral analysis package CLIMAX.[52] The mean-square atomic displacements, as calculated by CLIMAX and weighted by the atom's incoherent scattering cross section, are directly related to the reported intensities, $S(Q,\omega)$. The cross section of hydrogen, 80 barns, is much larger than for any other atom and the observed INS spectrum of hydrogenous material is dominated by hydrogen displacements. The CLIMAX program also performs several important, but nowadays straightforward, calculations which permit direct comparison of the observed and calculated INS spectra. These calculations have been discussed elsewhere[52,54] and only the role of "phonon wings" needs outlining here. These are combinations between the internal and the external, or lattice, vibrations of the molecule. They become active whenever significant momentum transfer, Q, is involved when exciting the transition. Because of the neutron's mass, momentum transfer is always implied. However, they are also visible in the optical spectra of molecular impurities in crystals, where the restriction to the Brillouin zone centre is raised. In our case the wings appear to the high-energy side of the internal transition. The relative intensity of the wing, S_W, to the intensity remaining at the band origin, S_O, depends on the mean-square displacement of the scattering atom due to the external vibrations, U_E^2. INS therefore gives access to the individual internal vibrational displacements (U^2) through the total intensity observed in a band (S_T), as well as to the external displacements, through the intensity of its phonon wing. The total atomic displacement, U_T^2, determined in this manner is the same as

TABLE 1: Bond Lengths (Å) and Bond Angles (deg)

internal coordinates	$H_8Si_8O_{12}$	$H_{10}Si_{10}O_{15}$
R(Si−H)	1.48	1.48
r(Si−O)	1.62	1.61
s(Si−O)		1.60
α(O−Si−H)	109.5	109.5
β(O−Si−O)	109.5	109.5
γ(O−Si−H)		109.5
δ(O−Si−O)		109.5
Φ(Si−O−Si)	148.4	150.5
Ψ(Si−O−Si)		156.1

SCHEME 1: Structure and Internal Coordinates of $H_8Si_8O_{12}$ and $H_{10}Si_{10}O_{15}$

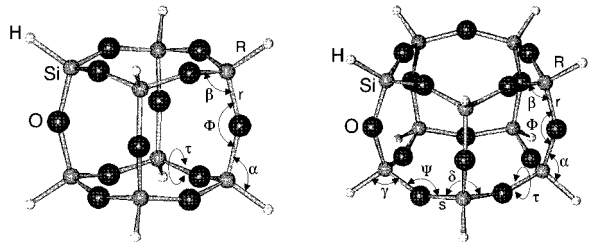

that measured by diffraction techniques, provided that there is no static disorder in the crystal.

The structure and definition of the internal coordinates of $H_8Si_8O_{12}$ and $H_{10}Si_{10}O_{15}$ are shown in Scheme 1. The bond lengths and bond angles of O_h $H_8Si_8O_{12}$ and D_{5h} $H_{10}Si_{10}O_{15}$ used for the normal-coordinate analysis are reported in Table 1. The vibrational analysis of $H_8Si_8O_{12}$, $D_8Si_8O_{12}$, and $H_{10}Si_{10}O_{15}$ was based on the modified general valence force field from IR and Raman data of $H_8Si_8O_{12}$ and $D_8Si_8O_{12}$.[28] The experimental and the calculated fundamentals of $H_8Si_8O_{12}$ are reported in Table 2, and the force constants used are listed in Table 3. According to molecular symmetry (see Table 5 in ref 28), some of the internal force constants are linearly dependent and 3 of the 13 off-diagonal elements had to be eliminated. One way to solve this problem was to set $f_{\alpha\alpha}$, $f_{\beta\beta}$, and $f'_{r\alpha}$ equal to zero. The fits finally obtained were not sensitive to this procedure.

Crystal Structure and Symmetry

The structure of crystalline $H_8Si_8O_{12}$ was examined in detail by X-ray[42] and neutron[43] diffraction. Both techniques show S_6 (3) crystallographic symmetry and T_h symmetry for the Si_8O_{12} framework. The ideal O_h symmetry is only realized in solution, since the ^{1}H and ^{29}Si NMR spectra each consist of a single peak, and the IR spectrum of $H_8Si_8O_{12}$ is compatible with the O_h point group.[28] The clearest manifestation of the T_h molecular symmetry in the crystal is the difference between the O···O distances across the faces of the Si_8 cube (∼0.31 Å). The symmetry lowering actually originates from intermolecular interactions as revealed when inspecting the packing. Four relatively short O···Si contacts between each pair of molecules are observed. These have been interpreted as reminiscent of an incipient nucleophilic attack of O on Si.[42] Low-temperature neutron diffraction[43] located the H atom positions and showed that all Si−H distances are the same within experimental error. The symmetry reduction from O_h to S_6 leads to two sets of equivalent H atoms, the first set consisting of the two axial H(1) lying on the threefold axis, and the other one consisting of the six equatorial H(2) as shown in Scheme 2a. The deviation of the H(2) set of atoms from ideal tetrahedral angles (∠(O−Si−H): 109.86°, 109.07°, 109.77°) is caused by interatomic interaction.

TABLE 2: Fundamentals of $H_8Si_8O_{12}$

	experimental			calculated		
sym	IR[a]	Raman[b]	INS	I[c]	II[d]	type of vibration
A_{1g}		2302	2301	2290	2290	ν(Si−H)
T_{2g}		2286/2296	2301	2290	2290	
T_{1u}	2277		2301	2290	2290	
A_{2u}			2301	2290	2290	
T_{1g}				1161	1161	ν_{as}(Si−O−Si)
E_u				1158	1158	
T_{1u}	1141			1143	1142	
T_{2g}		1117		1116	1114/1113	
A_{2u}				1082	1079	
E_g		932	916	922	910	δ(O−Si−H)
T_{2u}			916	918	914/904	
T_{2g}		897/883	890/879	894	893/881	
T_{1u}	881		879/870	881	878/869	
T_{1g}		811	870/817	865	862/820	
E_u			817	862	818	
E_g		697	688	691	704	ν_s(Si−O−Si)
T_{2u}			675	682	692/690	
T_{2g}		610	608	613	617/614	
A_{1g}		580	563	576	553	δ(O−Si−O)
T_{1u}	566		563	569	569/561	ν_s(Si−O−Si)
T_{1u}	465		458	481	473/461	
A_{1g}		456	458	446	446	
E_g		423	415	423	422	δ(O−Si−O)
T_{2g}		414	405/400	418	407/397	
T_{1u}	399		389	397	400/390	
T_{1g}		352	330	356	361	
A_{2u}			314	304	303	
T_{2u}			286	303	301/290	
T_{2g}		171	178/175	168	168	
E_u			172	166	168	
E_g		84	88	83	83	δ(Si−O−Si)
T_{2u}			65	68	68	
A_{2g}					41±7	τ_{as}(Si−O−Si)

[a] In CCl_4. [b] Crystalline powder. [c] Calculated with the force field from ref 28. [d] Calculated with the force field adapted to $H_8Si_8O_{12}$ in the crystal.

TABLE 3: Internal Force Constants of $H_8Si_8O_{12}$

force const[a]	ref 28	this work	force const[a]	ref 28	this work
f_R	3.0	3.0	$f_{t\beta}$	−0.016	−0.016
f_r	5.10	5.10	$f'_{r\beta}$	0.144	0.144
f_α^{ax}		0.606	$f_{r\Phi}$	0.036	0.036
f_α^{eq}	0.601	0.533	$f_{\alpha\alpha}$	0	0
f_β	0.895	0.895	$f_{\beta\beta}$	0	0
f_Φ	0.091	0.091	$f_{\alpha\beta}$	−0.095	−0.095
f_{rr}	0.275	0.275	$f'_{\alpha\beta}{}^{ax}$	−0.175	0
f'_{rr}	0.153	0.153	$f'_{\alpha\beta}{}^{eq}$		−0.109
$f_{r\alpha}$	0.188	0.188	$f_{\alpha\Phi}$	0.0188	0.0188
$f'_{r\alpha}$	0	0	$f_{\beta\Phi}$	0.0026	0.0026

[a] Force constants units: stretching constants, mdyn/Å; bending constants, mdyn Å/rad^2; stretch bend interactions, mdyn/rad.

SCHEME 2: Symmetry of $H_8Si_8O_{12}$ (a) and $H_{10}Si_{10}O_{15}$ (b) in the Crystal

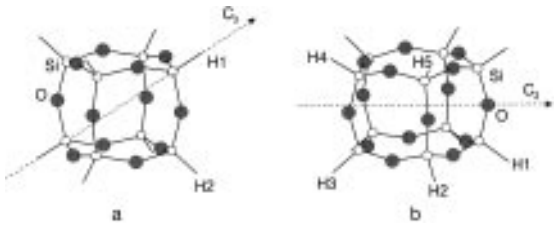

Analysis of the O···H distances between neighboring molecules in the crystal showed three short O···H(1) distances (2.942 Å) and one rather short O···H(2) distance (3.023 Å); see Figure 1.

The deviations from the ideal O_h symmetry are small and the spectra measured in solution are fully compatible with this symmetry. Therefore, the vibrations are described within the

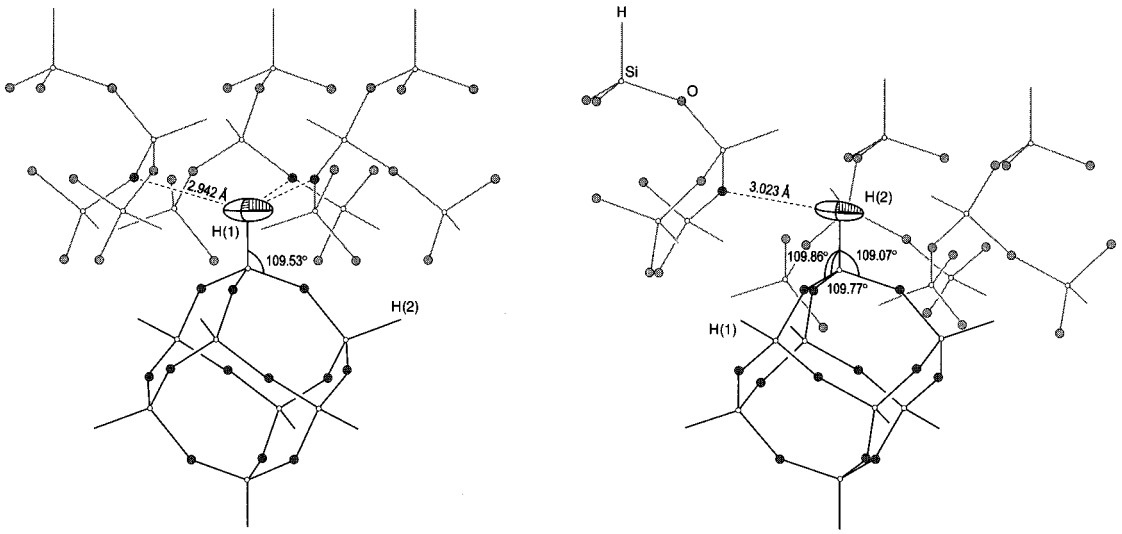

Figure 1. H(1) atom (on the left-hand side) and H(2) atom (on the right-hand side) of $H_8Si_8O_{12}$ as located in the crystal with RMS amplitudes from neutron diffraction (the shortest H···O distances are indicated).

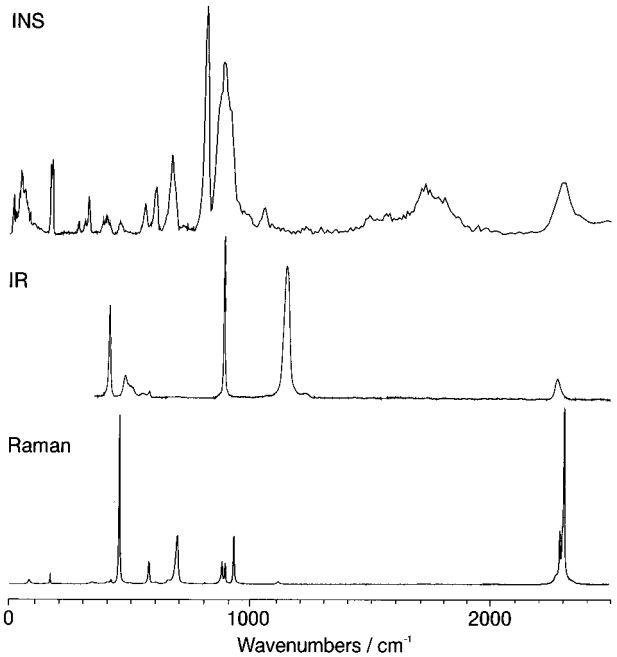

Figure 2. INS and Raman spectra of crystalline $H_8Si_8O_{12}$ and IR transmission spectrum of the solution in CCl_4.

O_h point group and deviations from this symmetry are discussed separately. Based on O_h, the 78 vibrational degrees of freedom of $H_8Si_8O_{12}$ are distributed between the irreducible representations as follows:

$$\Gamma_{vib} = 3A_{1g}(R) + A_{2g}(in) + 4E_g(R) + 3T_{1g}(in) + 6T_{2g}(R) + 3A_{2u}(in) + 3E_u(in) + 6T_{1u}(IR) + 4T_{2u}(in)$$

Among the 33 different fundamental vibrations of O_h $H_8Si_8O_{12}$, 14 are optically inactive, but all should be INS active. The only limiting factors are the resolution of the INS technique and the intrinsic peak intensity, related to the hydrogen displacement present in a vibration of $H_8Si_8O_{12}$.

INS, IR, and Raman Spectra

Qualitative Comparison of the Spectra. The INS spectrum of $H_8Si_8O_{12}$ is shown together with the optical (IR and Raman) spectra in Figure 2, and the frequencies of the fundamentals are listed in Table 2. The IR spectrum, which was taken from the solution, can be strictly understood in terms of O_h symmetry. It consists of the six IR active T_{1u} modes and four combination or difference bands. Though the Raman spectrum shown in Figure 2 was taken from the solid, most features can be understood in terms of O_h symmetry. Thirteen vibrations are Raman active in O_h symmetry and can be without exception assigned to peaks in the Raman spectrum. Additional peaks, which are of low intensity in comparison with the Raman active fundamentals, are assigned to combination bands or to fundamentals activated by symmetry reduction in the crystal. A detailed discussion of these spectra can be found in refs 28 and 34. The influence of the symmetry reduction in the crystal is most apparent for vibrations involving hydrogen atoms. We therefore compare in Figure 3 the O−Si−H bending and the Si−H stretching region of the Raman spectra of solid and dissolved (cyclohexane) $H_8Si_8O_{12}$. Solid samples show a splitting of the triply degenerate T_{2g} modes. Thus, the T_{2g} Si−H stretching vibration is split into a doublet (A_g and E_g) at 2296 and 2286 cm^{-1} and the T_{2g} O−Si−H bending vibration into a doublet at 883 and 897 cm^{-1}. In addition to these splittings, shifts to higher wavenumbers are observed in the crystal. In solution the T_{2g} (2275 cm^{-1}) and the A_{1g} (2281 cm^{-1}) modes are detected at 20 cm^{-1} lower energy than in the crystal, close to the position of the T_{1u} ν(Si−H) (2277 cm^{-1}) in the IR spectrum. A similar shift is observed for the E_g O−Si−H bending mode, which appears for the solid at 15 cm^{-1} higher energy than for the solution.

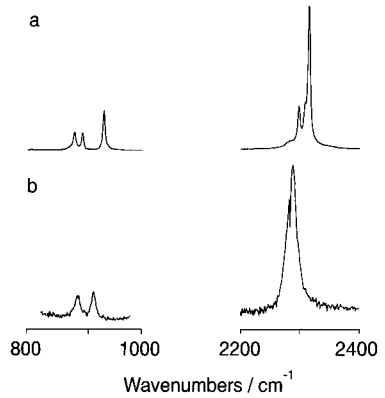

Figure 3. Raman spectra of the solid (a) and of the solution in cyclohexane (b) of the Si−H stretching and O−Si−H bending region.

The INS spectrum of $H_8Si_8O_{12}$ should include the six IR and 13 Raman active as well as the 14 inactive vibrations. Inspec-

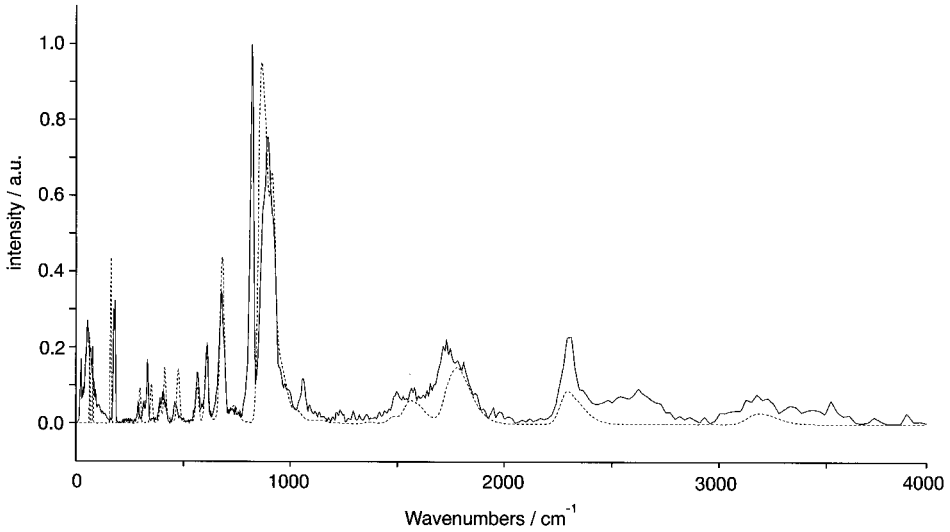

Figure 4. Measured (straight line) and calculated (dotted line) INS spectra of $H_8Si_8O_{12}$. The calculation was carried out with the same force constants as for the IR and Raman data.

tion of the INS spectrum shows that it is indeed the richest and consists of both broad and sharp features. The broad features are due to overlapping bands, overtones, and combinations. The fundamentals appear as sharp peaks (full width at half-height of 10−20 cm^{-1}) over the whole spectral range. All IR- or Raman-active fundamentals, with the exception of the antisymmetric Si−O−Si stretches, could be detected in the INS spectrum, and the comparison with the IR and Raman spectra shows agreement within about 10 cm^{-1}. This quality of agreement together with the fact that the bandwidth is comparable with the instrument resolution demonstrates that dispersion is irrelevant in $H_8Si_8O_{12}$. All optically inactive bands could be detected in the INS spectrum, again with the exception of the antisymmetric Si−O−Si stretches. Based on a potential energy distribution (PED) analysis,[28,53] the vibrations of $H_8Si_8O_{12}$ can be conveniently described as follows: ν(Si−H), ν_{as}(Si−O−Si), δ(O−Si−H), ν_s(Si−O−Si), δ(O−Si−O), δ(Si−O−Si). For a consistent assignment in terms of group frequencies, however, it was necessary to introduce the notion of ring opening vibrations.[34]

The Si−H stretching vibrations, ν(Si−H), are the highest fundamentals of $H_8Si_8O_{12}$. They are not resolved in the INS spectrum and appear as a single broad band at 2301 cm^{-1} (width, 80 cm^{-1}). In the Raman spectrum of the solid they appear at a similar position. Additional features, only observed in the INS spectrum, are the bands between 1200 and 2000 cm^{-1}. They are readily assigned to the first overtones and combinations of the O−Si−H bending motions. The antisymmetric Si−O−Si stretching region, ν_{as}(Si−O−Si) between 1000 and 1200 cm^{-1}, contributes only a weak band at 1059 cm^{-1}. Above 1100 cm^{-1}, where the IR- and Raman-active Si−O−Si stretches are detected no INS intensity was measured. This is not unexpected as these vibrations involve no displacement of the hydrogen atoms and are therefore of weak intensity. The whole INS spectrum is dominated by the two strong bands with maxima at 890 and 817 cm^{-1}. Because of their intensity and position they are assigned to O−Si−H bending vibrations. Under O_h symmetry six O−Si−H bending modes are expected; one of them is IR active, two are Raman active, with three optically inactive modes. While, because of its position the band at 890 cm^{-1} must contain the IR and the Raman active modes, the intense peak at 817 cm^{-1} consists of the optically inactive modes.

Between 100 and 800 cm^{-1} the symmetric Si−O−Si stretches (750−550 cm^{-1}) and the O−Si−O bending vibrations (500−150 cm^{-1}) occur. Fifteen vibrations are expected for O_h $H_8Si_8O_{12}$ in this region: three IR active, seven Raman active, and five inactive. All optically inactive vibrations are detected in the INS spectrum and the assignment is given in Table 2. The T_{1g} δ(O−Si−O) is Raman inactive in O_h symmetry but becomes active in S_6 symmetry. It appears as a weak Raman peak at 356 cm^{-1} in the crystalline material and is observed at 330 cm^{-1} in the INS spectrum and displays the largest wavenumber difference between the Raman and the INS spectrum for solid $H_8Si_8O_{12}$. In the range from 490 to 390 cm^{-1} the ring-opening vibrations occur, which give rise to characteristic IR and Raman bands, mainly to the strong and totally symmetric Raman peak at 456 cm^{-1}. The INS spectrum of the ring-opening modes is weak as only small hydrogen displacements are involved in these vibrations. They are partly responsible for the intensities of the peaks located at ca. 400 and 458 cm^{-1}.

The TFXA spectrometer provides access down to about 20 cm^{-1}, covering the external or lattice mode region below 100 cm^{-1}. The INS spectrum in this region is a broad but structured feature between 30 and 100 cm^{-1} and reaches a maximum at 50 cm^{-1}. Three internal modes are also expected in this region and one of them, the E_g δ(Si−O−Si), is observed in the Raman spectrum at 84 cm^{-1}, but the other two, the T_{2u} δ(Si−O−Si) and the A_{2g} torsion, are still to be firmly located.

Force Field. The force field determined from the IR and Raman data of $H_8Si_8O_{12}$ and $D_8Si_8O_{12}$[28] was used together with the high-symmetry geometry (O_h, Table 1) as input to the INS analysis program CLIMAX.[54] The experimentally available information imposed a restricted number of interaction force constants (Table 3). Indeed, most interactions which were not between coordinates within the same $HSiO_3$ tetrahedron were neglected. Figure 4 demonstrates that this force field provides a good fit of the observed neutron features over the whole spectral range with the exception of the strong peak at 817 cm^{-1} and the weak feature at 1059 cm^{-1}, which are both missing from the calculated spectrum. This agreement confirms that the dynamics of $H_8Si_8O_{12}$ can be well described by flexibly jointed $HSiO_3$ units with C_{3v} symmetry. Intensity is also missing in the frequency region below 100 cm^{-1}, indicating that the intensity in this region stems mainly from external modes. The CLIMAX calculation shown in Figure 4 includes overtones and combinations to first order and is therefore able to fit the first overtones and combinations of the O−Si−H bending vibrations between 1200 and 2000 cm^{-1}. The broad feature above 3000 cm^{-1} arises from the combination bands of the Si−H stretching and the O−Si−H bending modes. The

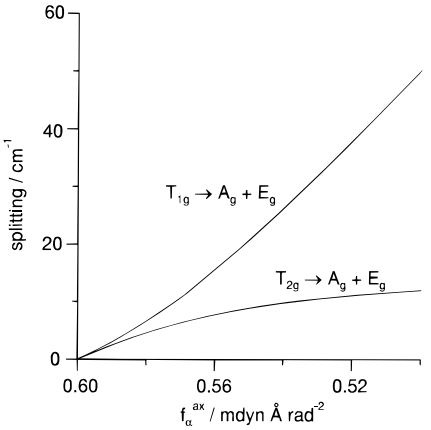

Figure 5. Splitting of the T_{1g} δ(O−Si−H) (at 865 cm^{-1} for O_h $H_8Si_8O_{12}$) and the T_{2g} δ(O−Si−H) (at 894 cm^{-1} for O_h $H_8Si_8O_{12}$) modes as a function of f_α^{ax}.

intensity observed in the region between 2100 and 2800 cm^{-1} underlying the Si−H stretch at 2300 cm^{-1} is due to second-order combinations and overtones of the O−Si−H deformation modes and does not appear in the calculated spectrum.

To explain the discrepancies between the calculated and the observed spectrum of $H_8Si_8O_{12}$ in the O−Si−H bending region of Figure 4, the reduced symmetry of the crystal was taken into account. It can be seen from the Raman spectrum that the intermolecular interactions, due to the relatively short O···H distances in the crystal, lead to considerable splitting in the O−Si−H bending and in the Si−H stretching regions. The CLIMAX calculation was repeated with the same force constants as previously but with the atomic coordinates as determined by neutron diffraction. However, this led only to small changes in the spectrum and could not reproduce the splitting observed in the Raman spectrum. We therefore renounced replacing the idealized coordinates by the true atomic positions and focused on the force constant values.

The crystal geometry S_6 together with the relatively short O···H contacts between neighboring molecules imply that the force constants of the axial hydrogen atoms, H(1) can have different values from their equatorial counterparts, H(2). We therefore distinguished between the O−Si−H bending force constants of the H(1), f_α^{ax}, and the H(2), f_α^{eq}. The results of the systematic investigation of varying f_α^{ax} are shown in Figure 5; the splitting of T_{2g} δ(O−Si−H) and T_{1g} δ(O−Si−H) are plotted as a function of f_α^{ax} (f_α^{eq} remained fixed at 0.60 mdyn Å rad^{-2}). It is seen that both modes split into A_g and E_g components. The splitting of the T_{1g} δ(O−Si−H) is always greater than that of the T_{2g} δ(O−Si−H). At $f_\alpha^{ax} = 0.50$ mdyn Å rad^{-2} this splitting is 50 cm^{-1}, while for the T_{2g} δ(O−Si−H) mode is similar to that observed in the Raman spectrum, i.e., about 13 cm^{-1}. In addition, the optically inactive E_u δ(O−Si−H) is shifted down by 50 cm^{-1}. *This means that differentiating between f_α^{ax} and f_α^{eq} leads to the splitting of the T_{2g} δ(O−Si−H) experimentally observed in the Raman spectrum of the crystal as well as to the appearance of the O−Si−H bending modes as two distinct features in the INS spectrum.* A similar distinction between the axial and the equatorial Si−H stretching force constants leads to the splitting of the T_{2g} ν(Si−H), which is observed in the Raman spectrum of crystalline $H_8Si_8O_{12}$. Based on Figure 5, approximate magnitudes for f_α^{ax} and f_α^{eq} were estimated and used as initial values for a fit to the INS spectrum using CLIMAX. The best fit to the INS intensities was obtained when the distinction between $f'_{\alpha\beta}{}^{ax}$ and $f'_{\alpha\beta}{}^{eq}$, analogous to that between f_α^{ax} and f_α^{eq}, was introduced. Only the $f'_{\alpha\beta}{}^{eq}$, f_α^{ax}, and f_α^{eq} force constants were allowed to vary during the fit. The finally accepted force field is given in Table 3 and the calculated spectrum is shown in Figure 6a in the region from 500 to 1200 cm^{-1}.

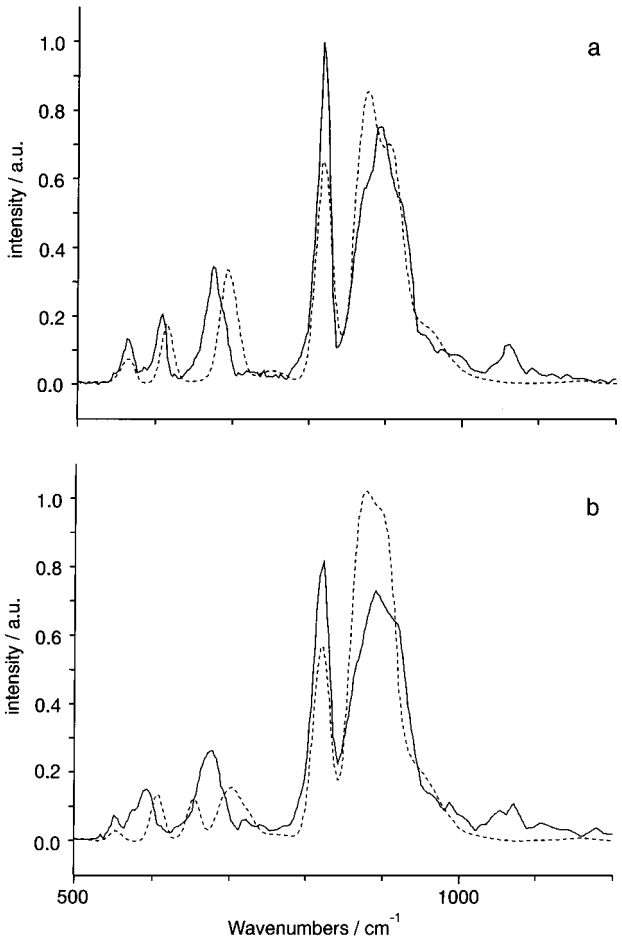

Figure 6. Measured (straight line) and calculated (dotted line) INS spectra of $H_8Si_8O_{12}$ (a) and $H_{10}Si_{10}O_{15}$ (b). The calculation was carried out with different values for nonequivalent O−Si−H bending force constants as reported in Table 3.

It can be seen that the fit is much improved in the O−Si−H bending region, which now displays two strong bands. In Table 2, column II, the frequencies are listed, showing a considerable splitting for all triply degenerate O−Si−H bending vibrations. The restricted number of variables and the CLIMAX fitting procedure, which optimizes both INS intensities and positions, made the frequency agreement for the 675 cm^{-1} band worse. Nevertheless, this is acceptable to obtain a good INS intensity agreement with frequencies remaining as close as possible to the earlier force field of ref 28. The weak but sharp feature at 1059 cm^{-1} assigned to the lowest ν_{as}(Si−O−Si) mode (A_{2u} character) is not well represented by the calculated spectrum. This mode only has intensity by virtue of interactions with hydrogen modes of other character. The interaction with the O−Si−H bending modes, as they contain no vibration of A_{2u} symmetry, is absent for O_h $H_8Si_8O_{12}$ but becomes active in the lower S_6 point group. To account for this peak in the calculated spectrum, a more explicit treatment of the intermolecular interactions in the crystal would be necessary.

Overtones and Combinations. The additional features in the INS spectrum above 1200 cm^{-1} originate from overtones and combination bands, which are known to give much more intense features in the INS spectrum than in the corresponding optical spectra. Although only first-order overtone and combination processes are calculated in CLIMAX, their relative intensities are in good agreement with observation.

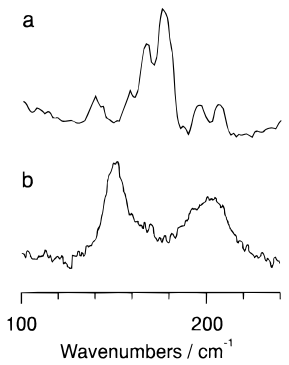

Figure 7. Comparison of the INS (a) and the Raman spectrum (b) of $H_{10}Si_{10}O_{15}$ in the low-frequency region. The INS spectrum shows two splittings not observed in the Raman spectrum.

$H_{10}Si_{10}O_{15}$. The modified general valence force field determined for O_h $H_8Si_8O_{12}$ proved to be readily transferable to $H_{10}Si_{10}O_{15}$ and led to an accurate description of the IR and Raman data.[34] When applied to the INS spectrum of crystalline $H_{10}Si_{10}O_{15}$, we found the same discrepancies in the O−Si−H bending region as for $H_8Si_8O_{12}$. This indicates that the force constants describing the dynamics of the hydrogen atoms in $H_{10}Si_{10}O_{15}$ show a similar dependence on the molecular packing as those of $H_8Si_8O_{12}$. Indeed X-ray analysis shows similar situations for both crystals, with a symmetry reduction to C_2 for $H_{10}Si_{10}O_{15}$.[44] However, the solution IR spectrum is fully compatible with a D_{5h} symmetry.[34] Considerable deviations from ideal D_{5h} symmetry have been attributed to relatively short O···Si contacts on packing eight- and ten-membered rings. The O···H distances between neighboring $H_{10}Si_{10}O_{15}$ molecules, calculated with Si−H distances of 1.48 Å and O−Si−H angles of 109.1°, are of the same order as in $H_8Si_8O_{12}$. With C_2 symmetry the H atoms form five sets of equivalent atoms, as shown in Scheme 2b. The shortest O···H distances are measured for H(2), where the closest oxygen contact (2.636 Å) lies on the prolongation of the Si−H bond axis. The influence of molecular packing is also observed in the Raman spectra of $H_{10}Si_{10}O_{15}$. A comparison of the Raman spectra of dissolved and solid materials shows a shift to higher wavenumber for the Si−H stretches in the solid and splittings in the O−Si−H bending region. We therefore applied the force field developed above to crystalline $H_{10}Si_{10}O_{15}$. For H(2) the values of f_α^{ax} and $f'_{\alpha\beta}{}^{ax}$ were used and for the other H atoms, the values of f_α^{eq} and $f'_{\alpha\beta}{}^{eq}$ are those listed in Table 3. Figure 6b shows the fit between 500 and 1200 cm^{-1}. The main features in the O−Si−H bending region are described correctly but the intensity distribution between the split peaks (here 889 and 822 cm^{-1}) is less satisfactory than for $H_8Si_8O_{12}$. Although the situation in $H_{10}Si_{10}O_{15}$ is more complex, the description in terms of the limited number of interaction constants is correct and suggests that similar forces are active in both crystals.

Figure 7 shows a part of the low-frequency region of the INS (a) and the Raman (b) spectrum of $H_{10}Si_{10}O_{15}$. The bands at 168 and 176 cm^{-1} in the INS spectrum are Raman inactive. Interestingly, the E'_2 δ(O−Si−O) and the E''_1 δ(O−Si−O) at 202 and 152 cm^{-1}, respectively, in the Raman spectrum of $H_{10}Si_{10}O_{15}$, appear as doublets in the INS spectrum. The CLIMAX calculation of $H_{10}Si_{10}O_{15}$ was carried out (using the force constants determined from $H_8Si_8O_{12}$) with the two sets of atomic coordinates available from X-ray data, one measured at 180 and the other at 295 K. Although both led to splittings below 700 cm^{-1}, these are larger with the 180 K coordinates. The band at ca. 200 cm^{-1} (E'_2 δ(O−Si−O)) shows at 295 K a splitting of 2 cm^{-1} and at 180 K a splitting of 4 cm^{-1}. For E''_1 δ(O−Si−O), measured as a doublet at 141 and 158 cm^{-1} in the INS spectrum, the splitting of 2 cm^{-1} at 295 K is increased to 5 cm^{-1} at 180 K. Routine X-ray monitoring of the crystal during cooling revealed a reversible phase change for $H_{10}Si_{10}O_{15}$ between 155 and 165 K.[44] We attribute differences in the magnitude of the splittings as seen by INS and Raman spectrum to the different measuring temperatures.

TABLE 4: Total Mean-Square Displacements (msd's) along the Principal Axes/Å²

	INS	neutron diffraction[a]
H(1)		
$\perp_{Si-H}$	0.0279 (5)[b]	0.0273 (15)
$\|\|_{Si-H}$	0.0136 (5)[b]	0.0122 (15)
H(2)		
$\perp_{Si-H}$	0.0267 (5)[b]	0.0262 (10)
$\|\|_{Si-H}$	0.0135 (5)[b]	0.0087 (10)
Si(1), isotropic	0.0045 (5)[c]	0.0049 (5)
	0.0063 (5)[d]	
Si(2), isotropic	0.0045 (5)[c]	0.0048 (3)
	0.0063 (5)[d]	

[a] Reference 43. [b] Calculated with an external contribution of 0.0050 (5) Å². [c] Lower limit, calculated with external contribution for the purely librational case (0.0032 (5) Å²). [d] Upper limit, calculated with external contribution for the purely translational case (0.0050 (5) Å²).

$D_8Si_8O_{12}$. $D_8Si_8O_{12}$ gives a much noisier INS spectrum than the hydrido derivatives because of two reasons. First, the deuterium scattering cross section is smaller than for hydrogen (a factor 20) and, second, only 340 mg was available. However, within the limits of available data, the force field reported in Table 3 was found to be in good agreement with this spectrum.

Total Mean-Square Displacements. The interpretation of the total mean-square displacements (msd), a parameter routinely obtained from crystal structure analysis, is often difficult because numerous kinds of disorder (static and dynamic) are responsible for the observed atomic displacements in a crystal. The INS technique offers an alternative possibility of calculating a value for the total msd's of hydrogen, which only includes the dynamic contributions. This value is composed of an internal component, which is a result of the normal-coordinate analysis, and an external component provided by the CLIMAX evaluation of the phonon wings (typical features of the INS spectra, as discussed earlier). We can therefore compare the total msd's of the hydrogen atoms as determined by inelastic and elastic experiments. For the silicon atoms the external contribution to the total msd is not directly accessible; however, it can be calculated for the two limiting cases of purely librational and purely translational external contributions.

The contribution from the external hydrogen displacements of $H_8Si_8O_{12}$ was estimated by fitting the phonon wing of the strongest feature namely the O−Si−H bending vibrations. The value thus obtained, 0.0050 (5) Å², was added to the internal vibrational contribution to provide the total msd's of the hydrogen atoms. Since the INS (7 K) and diffraction[43] (29 K) measurements were performed at similar temperatures, a direct comparison is now possible. The total msd's reported in Table 4 refer to a principal axis system where $\perp_{Si-H}$ is perpendicular and $||_{Si-H}$ parallel to the Si−H bond. This axis system is appropriate for the H(1) set but only approximate for the H(2) set, which has a deviation of 4°.[55] We observe excellent agreement of the hydrogen total msd's, perpendicular to the Si−H bond. The neutron diffraction values, parallel to the Si−H bond, are significantly smaller than the INS values and show a considerable difference between H(1) and H(2), which is not observed in our INS estimate. These discrepancies are partly due to the "isotropic" approximations used in the CLIMAX calculations and also to the fitting of a single parameter for all

types of atoms. The size of the differences between the H(1) and H(2) displacements (from diffraction data) cannot be attributed to different Si−H stretching contributions, since these coordinates give rise to very small contributions to the atomic displacements.

Because the external contribution to the total msd's of the silicon atoms is not directly accessible from our INS spectra, we evaluate it from the external components of the hydrogen atom displacements for two limiting cases, i.e., the purely translational and the purely librational. In the purely translational case the external displacements of hydrogen and silicon atoms are the same (0.0050 (5) Å^2). For the librational case the shorter radius of gyration of the silicon atoms must be taken into consideration, leading to a silicon external displacement of 0.0032 (5) Å^2. In Table 4 the values for these two limiting cases are added to the internal contribution to give an estimate of the total msd's, which can be compared with those given by the diffraction study. We see that the total msd's measured by diffraction are within the limits given by the two cases of purely librational and purely translational external motions. The total msd's of silicon atoms are dominated by the external displacements. This is in sharp contrast to the hydrogen displacements and reflects the disparity of the atomic masses. The accuracy of our estimated silicon displacements is therefore limited by the approximations used to extract the external displacements for hydrogen atoms. We conclude that the normal-coordinate analysis is in agreement with the diffraction data and leads to an accurate description of the internal displacements of the silicon atoms. This good agreement reflects the soundness of our approach and the quality of the reported force field.

Torsion. O_h $H_8Si_8O_{12}$ has one A_{2g} torsional vibration which is optically inactive but anticipated to be its lowest lying fundamental mode. This torsion is simultaneously about all Si−H bonds and involves predominantly a motion of the oxygen atoms. Because it includes very little hydrogen motion it is expected to be weak in the INS spectrum. This is confirmed by the CLIMAX analysis which calculated it as a very weak feature in the external region, assuming any reasonable value for f_τ. Although we have no direct access to this torsional frequency we can estimate it by making use of its contribution to the total msd's. This procedure is meaningful because of the good agreement between the INS and the diffraction results for both H and Si atoms, and because the torsional contribution to the total msd of the oxygen atoms is expected to be significantly larger than the errors of measurement. Instead of calculating oxygen displacements in absolute terms the extra displacements of oxygen compared to silicon were evaluated. We thus took advantage of the similarity between the radii of gyration of O and Si to suppress contributions arising from the external displacements. The extra displacement of oxygen compared to silicon atoms was determined by evaluating the difference of the $\mathbf{U}_O$ and $\mathbf{U}_{Si}$ traces, $[\mathrm{Tr}(\mathbf{U}_O) - \mathrm{Tr}(\mathbf{U}_{Si})]$, where $\mathbf{U}$ is the anisotropic displacement tensor. Based on the mean-square displacements determined by the normal-coordinate analysis, $[\mathrm{Tr}(\mathbf{U}_O) - \mathrm{Tr}(\mathbf{U}_{Si})]_{spec}$ was calculated as a function of the torsional frequency at 29 K, as shown in Figure 8. These values were compared with $[\mathrm{Tr}(\mathbf{U}_O) - \mathrm{Tr}(\mathbf{U}_{Si})]_{diff}$ determined by diffraction (averaged over atom types 1 and 2) and indicated in the figure by the bold arrow. Figure 8 shows that the value of $[\mathrm{Tr}(\mathbf{U}_O) - \mathrm{Tr}(\mathbf{U}_{Si})]_{diff}$, 0.0095 (9) Å^2, corresponds to an A_{2g} torsional frequency of 41 ± 7 cm^{-1} (the calculation was repeated with the X-ray diffraction data measured at 100 K, leading to a very similar value of 42 ± 2 cm^{-1}). These values are in agreement with a rigid body analysis of X-ray data, which indicated a value of 49 cm^{-1} ($\pm\sigma$ region: 42−63 cm^{-1}).[32]

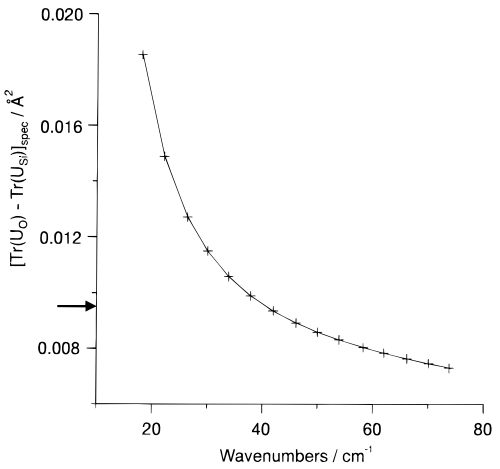

Figure 8. Difference of the $\mathbf{U}_O$ and $\mathbf{U}_{Si}$ traces $[\mathrm{Tr}(\mathbf{U}_O) - \mathrm{Tr}(\mathbf{U}_{Si})]_{spec}$ as a function of the torsional frequency. The bold arrow indicates the value of $[\mathrm{Tr}(\mathbf{U}_O) - \mathrm{Tr}(\mathbf{U})_{Si})]_{diff}$ corresponding to 0.0095 (9) Å^2.

Concluding Remarks

Based on INS, IR, and Raman data and on a normal-coordinate analysis, a detailed study of the vibrational structure of the silasesquioxanes $H_8Si_8O_{12}$ and $H_{10}Si_{10}O_{15}$ was presented. INS spectroscopy was used to locate the optically inactive vibrations of the highly symmetric $H_8Si_8O_{12}$. A comparison of the spectra taken from the crystalline solid (Raman and INS) and the solution (IR and Raman) showed the influence of the crystal packing, which is strongest in the O−Si−H bending region with splittings up to 50 cm^{-1}. Similar splittings as in $H_8Si_8O_{12}$ were also found for the O−Si−H bending vibrations of crystalline $H_{10}Si_{10}O_{15}$. This indicates that analogous forces are active in both crystals. A force field adapted to the crystalline solid, with different O−Si−H bending force constants for nonequivalent hydrogen atoms, provided a good fit of the INS frequencies and intensities in the whole spectral range, including the O−Si−H bending region. This good agreement confirms that the dynamics of $H_8Si_8O_{12}$ and $H_{10}Si_{10}O_{15}$ are in first order well described by a restricted set of interaction force constants, which includes mainly coordinates within the same $HSiO_3$ tetrahedron.

Based on the normal-coordinate analysis, values for the total mean-square displacements of the hydrogen atoms were extracted. The good agreement with the values determined by diffraction showed that none or very little static disorder is present in crystalline $H_8Si_8O_{12}$. The total mean-square displacements as determined by inelastic and elastic experiments were compared to provide a value of the lowest internal torsional frequency, τ_{as}: 41 ± 7 cm^{-1}.

It is worth noting that the dynamics of $(SiO_{3/2}H)_8$ should relate not only to higher order polyhedra, like $(SiO_{3/2}H)_{10}$, but also silica. In silica of course the terminal hydrogen atoms are replaced by bridging oxygen atoms, the regularity collapses, and a glass is formed. The assignment of the A_{2g} to 40 cm^{-1} underlines this relationship since it is precisely in this region of the spectrum that the equivalent oscillation of SiO_4 units were observed in silica.[56] Furthermore, it allows us to suggest that the oscillation occurring in silica is highly localized and might be fruitfully studied by using $H_8Si_8O_{12}$ as a model fragment of glass.

Acknowledgment. This work was supported by the Schweizerischer Nationalfonds zur Förderung der wissenschaftlicher Forschung (Project NF 20-040598.94/1). We thank the EPSRC for access to the neutron beams and the staff at

ISIS for all their help and support during the experiment, Prof. R. Giovanoli staff for thermal gravimetric analysis (TGA) and differential thermal analysis (DTA), and Dr. R. Imhof for fruitful discussions.

References and Notes

(1) Loy, D. A.; Shea, K. J. *Chem. Rev.* **1995**, *95*, 1431.
(2) Currently also named oligosilsesquioxanes or *spheros*iloxanes for topological reasons.
(3) Voronkov, M. G.; Lavrent'yev, V. I. *Top. Curr. Chem.* **1982**, *102*, 199.
(4) Baney, R. H.; Itoh, M.; Sakakibara, A.; Suzuki, T. *Chem. Rev.* **1995**, *95*, 1409.
(5) Calzaferri, G. *Proc. Taylor-Made Silicon-Oxygen Compounds, Mol. Mater., Bielefeld, Sept. 3*−*5, 1995* **1996**, 149.
(6) Bürgy, H.; Calzaferri, G.; Herren, D.; Zhdanov, A. *Chimia* **1991**, *45*, 3.
(7) Hoebbel, D.; Pitsch, I.; Heidemann, D. *Z. Anorg. Allg. Chem.* **1991**, *592*, 207.
(8) Agaskar, P. A. *J. Am. Chem. Soc.* **1989**, *111*, 6858.
(9) Agaskar, P. A. *Inorg. Chem.* **1990**, *29*, 1603.
(10) Harrison, P. G.; Kannengiesser R. *J. Chem. Soc., Chem. Commun.* **1996**, 415.
(11) Day, V. W.; Klemperer, W. G.; Mainz, V. V.; Millar, D. M. *J. Am. Chem. Soc.* **1985**, *107*, 8262.
(12) Bassindale, A. R.; Gentle, T. E. *J. Mater. Chem.* **1993**, *3*, 1319.
(13) Harrison, P. G.; Kannengiesser R. *J. Chem. Soc., Chem. Commun.* **1995**, 2065.
(14) Morán, M.; Casado, C. M.; Cuadrado I.; Losada, J. *Organometallics* **1993**, *12*, 4327.
(15) Desu, S. B.; Peng, C. H.; Shi, T.; Agaskar, P. A. *J. Electrochem. Soc.* **1992**, *139*, 2682.
(16) Nyman, M. D.; Desu, S. B.; Peng, C. H. *Chem. Mater.* **1993**, *5*, 1636.
(17) Bürgy, H.; Calzaferri, G. *Helv. Chim. Acta* **1990**, *73*, 698.
(18) Herren, D.; Bürgy, H.; Calzaferri, G. *Helv. Chim. Acta* **1991**, *74*, 24.
(19) Calzaferri, G.; Herren, D.; Imhof, R. *Helv. Chim. Acta* **1991**, *74*, 1278.
(20) Calzaferri, G.; Imhof, R. *J. Chem. Soc., Dalton Trans.* **1992**, 3391.
(21) Calzaferri, G.; Imhof, I.; Törnroos, K. W. *J. Chem. Soc., Dalton Trans.* **1993**, 3741.
(22) Marcolli, C.; Imhof, R.; Calzaferri, G. *Microchim. Acta* **1997**, Suppl. 14.
(23) Hendan, B. J.; Marsmann, H. C. *J. Organomet. Chem.* **1994**, *483*, 33.
(24) Dittmar, U.; Hendan, B. J.; Flörke, U.; Marsmann, H. C. *J. Organomet. Chem.* **1995**, *489*, 185.
(25) Nicholas, J. B.; Hopfinger, A. J.; Trouw, F. R.; Iton, L. E. *J. Am. Chem. Soc.* **1991**, *113*, 4792.
(26) Beagley, B.; Titiloye, J. O. *Struct. Chem.* **1992**, *3*, 429.
(27) Calzaferri, G.; Hoffmann, R. *J. Chem. Soc., Dalton Trans.* **1991**, 917.
(28) Bärtsch, M.; Bornhauser, P.; Calzaferri, G.; Imhof, R. *J. Phys. Chem.* **1994**, *98*, 2817.
(29) Harkless, J. A. W.; Stillinger, D. K.; Stillinger, F. H. *J. Phys. Chem.* **1996**, *100*, 1098.
(30) Ermoshin, V. A.; Smirnov, K. S.; Bougeard, D. *Chem. Phys.* **1996**, *202*, 53.
(31) de Man, A. J. M.; Sauer, J. *J. Phys. Chem.* **1996**, *100*, 5025.
(32) Bieniok, A. M.; Bürgi, H.-B. *J. Phys. Chem.* **1994**, *98*, 10735.
(33) Feher, F. J.; Newman, D. A.; Walzer, J. F. *J. Am. Chem. Soc.* **1989**, *111*, 1741.
(34) Bornhauser, P.; Calzaferri, G. *J. Phys. Chem.* **1996**, *100*, 2035.
(35) Murugavel, R.; Chandrasekhar, V.; Roesky, H. W. *Acc. Chem. Res.* **1996**, *29*, 183.
(36) Voigt, A.; Murugavel, R.; Parisini, E.; Roesky, H. W. *Angew. Chem., Int. Ed. Engl.* **1996**, *35*, 748.
(37) Montero, M.; Voigt, A.; Teichert, M.; Uśon, I.; Roesky, H. W. *Angew. Chem., Int. Ed. Engl.* **1995**, *34*, 2504.
(38) Feher, F. J.; Budzichowski, T. A.; Rahimian, K.; Ziller, J. W. *J. Am. Chem. Soc.* **1992**, *114*, 3859.
(39) Müller, A.; Reuter, H.; Dillinger, S. *Angew. Chem.* **1995**, *107*, 2505.
(40) Agaskar, P. A. *Inorg. Chem.* **1991**, *30*, 2707.
(41) Bürgy, H.; Calzaferri, G. *J. Chromatogr.* **1990**, *507*, 481.
(42) Auf der Heyde, T. P. E.; Bürgi, H.-B.; Bürgy, H.; Törnroos, K. W. *Chimia* **1991**, *45*, 38.
(43) Törnroos, K. W. *Acta Crystallogr.* **1994**, *C50*, 1646.
(44) Bürgi, H.-B.; Törnroos, K. W.; Calzaferri, G.; Bürgy, H. *Inorg. Chem.* **1993**, *32*, 4914.
(45) Törnroos, K. W.; Bürgi, H.-B.; Calzaferri, G.; Bürgy, H. *Acta Crystallogr.* **1995**, *B51*, 155.
(46) Agaskar, P. A.; Day, V. W.; Klemperer, W. G. *J. Am. Chem. Soc.* **1987**, *109*, 5554.
(47) Calzaferri, G.; Marcolli, C.; Imhof, R.; Törnroos, K. W. *J. Chem. Soc., Dalton Trans.* **1996**, 3313.
(48) Bürgy, H.; Calzaferri, G. *Helv. Chim. Acta* **1990**, *73*, 698.
(49) Penfold, J.; Tomkinson, J. RAL internal report **1986**, RAL-86-019.
(50) Wilson, E. B., Jr.; Decius, J. C.; Cross, P. C. *Molecular Vibrations*; McGraw-Hill Book Co. Inc.: New York, 1955.
(51) McIntosh, D. F.; Peterson, M. R. *General Vibrational Analysis System*; QCPE Program No. QCMP067, 1988.
(52) Kearley, G. J. *Nucl. Instrum. Methods* **1995**, *A354*, 53.
(53) Morino, Y.; Kuchitsu, K. *J. Chem. Phys.* **1952**, *20*, 1809.
(54) Kearley, G. J. *J. Chem. Soc., Faraday Trans. 2* **1986**, *82*, 41.
(55) The neutron diffraction data gives for the H(2) atoms two slightly different $\perp_{Si-H}$ values. For the purpose of comparison with our data an average value was adopted.
(56) Dianoux, A. J. *Philos. Mag.* **1989**, *B59*, 17.